Available online at www.sciencedirect.com
SCIENCE DIRECT®
International Journal of Heat and Fluid Flow 25 (2004) 196–208
International Journal of HEAT AND FLUID FLOW
www.elsevier.com/locate/ijhff

The influence of the bulk liquid thermal boundary layer on saturated nucleate boiling

Jun Liao, Renwei Mei *, James F. Klausner

Department of Mechanical and Aerospace Engineering, University of Florida, 231 Aerospace Building, P.O. Box 116250, Gainesville, FL 32611-6250, USA

Abstract

A physical model for vapor bubble growth in saturated nucleate boiling has been developed that includes both heat transfer through the liquid microlayer and that from the bulk superheated liquid surrounding the bubble. Both asymptotic and numerical solutions for the liquid temperature field surrounding a hemispherical bubble reveal the existence of a thin unsteady thermal boundary layer adjacent to the bubble dome. During the early stages of bubble growth, heat transfer to the bubble dome through the unsteady thermal boundary layer constitutes a substantial contribution to vapor bubble growth. The model is used to elucidate recent experimental observations of bubble growth and heat transfer on constant temperature microheaters reported by Yaddanapudi and Kim [Multiphase Sci. Technol. 12(3–4) (2001) 47] and confirms that the heat transfer through the bubble dome can be a significant portion of the overall energy supply for the bubble growth.

Keywords: Heat transfer; Nucleate boiling; Bubble growth

1. Introduction

During the past 40 years, the microlayer model has been widely accepted and used to explain bubble growth and the associated heat transfer in heterogeneous nucleate boiling. The microlayer concept was introduced by Moore and Mesler (1961), Labunstov (1963) and Cooper (1969). The microlayer is a thin liquid layer that resides beneath a growing vapor bubble. Because the layer is quite thin, the temperature gradient and the corresponding heat flux across the microlayer are high. The vapor generated by strong evaporation through the liquid microlayer substantially supports the bubble growth.

Popular opinion concerning the microlayer model is that the majority of evaporation takes place at the microlayer. A number of bubble growth models using microlayer theory have been proposed based on this assumption such as van Stralen et al. (1975a,b), Cooper and Vijuk (1970), and Fyodorov and Klimenko (1989). These models were partially successful in predicting the bubble growth under limited conditions but are not applicable to a wide range of conditions. Lee and Nydahl (1989) used a finite difference method to study bubble growth and heat transfer in the microlayer. However their model assumes a constant wall temperature, which is not valid for heat flux controlled boiling since the rapidly growing bubble draws a substantial amount of heat from the wall through the microlayer, which reduces the local wall temperature. Mei et al. (1995a,b) considered the simultaneous energy transfer among the vapor bubble, liquid microlayer, and solid heater in modeling bubble growth. For simplicity, the bulk liquid outside the microlayer was assumed to be at the saturation temperature so that the vapor dome is at thermal equilibrium with the surrounding bulk liquid. The temperature in the heater was determined by solving the unsteady heat conduction equation. The predicted bubble growth rates agreed very well with those measured over a wide range of experimental conditions that were reported by numerous investigators. Empirical constants to account for the bubble shape and microlayer angle were introduced.

Recently, Yaddanapudi and Kim (2001) experimentally studied single bubbles growing on a constant

* Corresponding author. Tel.: +1-352-392-0888; fax: +1-352-392-7303.
E-mail address: rwm@mae.ufl.edu (R. Mei).,

0142-727X/$ - see front matter © 2003 Elsevier Inc. All rights reserved.
doi:10.1016/j.ijheatfluidflow.2003.11.012

Nomenclature

A	dimensionless parameter for bubble growth
A_b	area of vapor bubble dome exposed to bulk liquid
A_m	area of wedge shaped interface
c	ratio of wedge shaped interface radius and vapor bubble radius
c_1	microlayer wedge angle parameter; empirically determined
d	bubble diameter
d_{eq}	equivalent bubble diameter
h_{fg}	latent heat of vaporization
k	thermal conductivity
L	local microlayer thickness
n	normal direction
R	vapor bubble radius
$\dot{R}$	bubble growth rate
R', ψ and φ	spherical coordinates
$\overline{R}'$	dimensionless radial coordinate
R_b	radius of wedge shaped interface
R_0	initial bubble radius
r	radial coordinate
$S_{\overline{R}'}$ and S_ψ	stretching factor in computation
T	temperature
T_{sat}	saturated temperature
T_w	initial solid temperature
T_b	bulk liquid temperature
t	time
t_c	characteristic time
t_w	waiting period
t_0	initial time
V_b	vapor bubble volume
X	boundary layer coordinate
Z	coordinate in the direction normal to the heating surface

Greeks

α	thermal diffusivity
ΔT_{sat}	solid heater superheat
δ	superheated bulk liquid thermal boundary layer thickness
δ^*	dimensionless thickness of unsteady thermal boundary layer
Φ	velocity potential function for liquid flow
ϕ	microlayer wedge angle
η and ξ	computational coordinates
ν	kinematic viscosity
θ	dimensionless temperature of liquid
θ_0	initial dimensionless temperature of liquid
ρ	density
σ	stretched time in computation
τ	dimensionless time

Superscripts

in	inner solution
out	outer solution

Subscripts

b	bubble
l	liquid
ml	microlayer
v	vapor
∞	far field condition

temperature heater. The heater temperature was kept constant by using electronic feed back loops, and the power required to maintain the temperature was measured throughout the bubble growth period. Their results show that during the bubble growth period, the heat flux from the wall through the microlayer is only about 54% of the total heat required to sustain the measured growth rate. It poses a new challenge to the microlayer theory since a substantial portion of the energy transferred to the bubble cannot be accounted for.

Since a growing vapor bubble consists of a thin liquid microlayer, which is in contact with the solid heater, and a vapor dome, which is in contact with the bulk liquid, the experimental observations of Yaddanapudi and Kim (2001) leads us to postulate that the heat transfer through the bubble dome may play an important role in the bubble growth process, even for saturated boiling. Because the wall is superheated, a thermal boundary layer exists between the background saturated bulk liquid and the wall; within this thermal boundary layer the liquid temperature is superheated. During the initial stage of the bubble growth, because the bubble is very small in size, it is completely immersed within this superheated bulk liquid thermal boundary layer. As the vapor bubble grows rapidly, a new unsteady thermal boundary layer develops between the saturated vapor dome and the surrounding superheated liquid. The thickness of the new unsteady thermal boundary layer should be inversely related to the bubble growth rate; see the asymptotic analysis that follows. Hence the initial rapid growth of the bubble, which results in a thin unsteady thermal boundary layer, is accompanied by a substantial amount of heat transfer from the surrounding superheated liquid to the bubble through the vapor bubble dome. This is an entirely different heat transfer mechanism than that associated with conventional microlayer theory.

In fact, many previous bubble growth models have attempted to include the evaporation through the bubble dome, such as Han and Griffith (1965) and van

Stralen (1967). However their analyses neglected the convection term in the bulk liquid due to the bubble expansion, so the unsteady thermal boundary layer was not revealed. This leads to a much lower heat flux through the bubble dome.

The existence and the analysis on the unsteady thermal boundary layer near the vapor dome were first discussed in Chen (1995) and Chen et al. (1996), when they studied the growth and collapse of vapor bubbles in subcooled boiling. For subcooled boiling, the effect of heat transfer through the dome is much more pronounced due to the larger temperature difference between the vapor and the bulk liquid. With the presence of a superheated wall, a subcooled bulk liquid, and a thin unsteady thermal boundary layer at the bubble dome, the folding of the liquid temperature contour near the bubble surface was observed in their numerical solutions. The folding phenomenon was experimentally confirmed by Mayinger (1996) using an interferometric method to measure the liquid temperature.

Despite those findings, the existence of the thin unsteady thermal boundary layer near the bubble surface has not received sufficient attention. In the recent computational studies of bubble growth by Son et al. (1999) and Bai and Fujita (2000), the conservation equations of mass, momentum and energy were solved in the Eulerian or Lagrange–Eulerian mixed grid system for the vapor–liquid two-phase flow. In their direct numerical simulations of the bubble growth process, the heat transfer from the surrounding liquid to the vapor dome is automatically included since the integration is over the entire bubble surface. They observed that there can be a substantial amount of heat transfer though bubble dome in comparison with that from the microlayer. However, it is not clear that if these direct numerical simulations have sufficiently resolved the thin unsteady thermal boundary layer that is attached to the rapidly growing bubble.

In this study, asymptotic and numerical solutions to the unsteady thermal fields around the vapor bubble are presented. The structure of the thin, unsteady thermal boundary layer around the vapor bubble is elucidated using the asymptotic solution for a rapidly growing bubble. A new computational model for predicting heterogeneous bubble growth in saturated nucleate boiling is presented. The model accounts for energy transfer from the solid heater through the liquid microlayer and from the bulk liquid through the thin unsteady thermal boundary layer on the bubble dome. It is equally valid for subcooled boiling, although the framework for this case has already been presented by Chen (1995) and Chen et al. (1996). The temperature field in the heater is simultaneously solved with the temperature in the bulk liquid. For the microlayer, an instantaneous linear temperature profile is assumed between the vapor saturation temperature and the heater surface temperature due to negligible heat capacity in the microlayer. For the bulk liquid, the energy equation is solved in a body-fitted coordinate system that is attached to the rapidly growing bubble with pertinent grid stretching near the bubble surface to provide sufficient numerical resolution for the new unsteady thermal boundary layer. Section 2 presents a detailed formulation of the present model and an asymptotic analysis for the unsteady thermal boundary layer. In Section 3, the experimental results of Yaddanapudi and Kim (2001) are examined using the computational results based on the present model. A parametric investigation considering the effect of the superheated bulk liquid thermal boundary layer thickness on bubble growth is also presented.

2. Formulation

2.1. On the vapor bubble

Consideration is given to an isolated vapor bubble growing from a solid heating surface into a large saturated liquid pool as shown in Fig. 1. A rigorous description of the vapor bubble growth and the heat transfer processes among three phases requires a complete account for the hydrodynamics around the rapidly growing bubble in addition to the complex thermal energy transfer. The numerical analysis by Lee and Nydahl (1989) relied on an assumed shape for the bubble, although the hydrodynamics based on the assumed bubble shape is properly accounted for. Son et al. (1999) and Bai and Fujita (2000) employed the Navier–Stokes equations and the interface capture or trace methods to determine the bubble shape. Nevertheless, the micro-

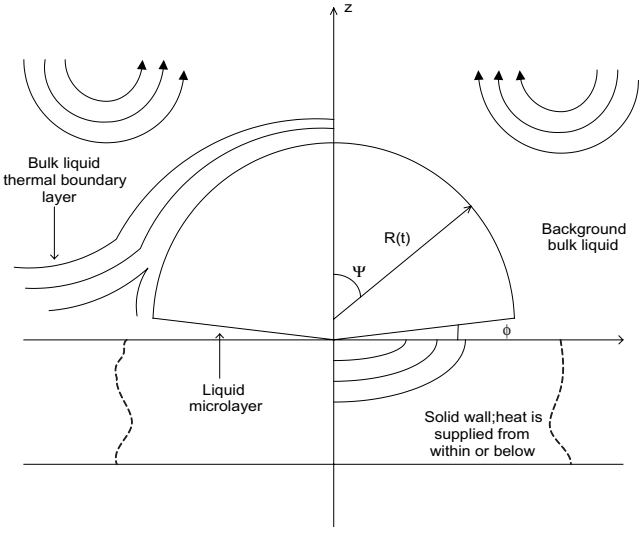

Fig. 1. Sketch for the growing bubble, thermal boundary layer, microlayer and the heater wall.

layer structure was still assumed based on existing models.

In this study, the liquid microlayer between the vapor bubble and the solid heating surface is assumed to have a simple wedge shape with an angle $\phi \ll 1$. The interferometry measurements of Koffman and Plesset (1983) demonstrate that a wedge shape microlayer is a good assumption. There exists ample experimental evidence by van Stralen et al. (1975a,b); Akiyama et al. (1969) that as a bubble grows, the dome shape may be approximated as a truncated sphere with radius $R(t)$, as shown in Fig. 1. Using cylindrical coordinates, the local microlayer thickness is denoted by $L(r)$. The radius of the wedge-shaped interface is denoted by $R_b(t)$, which is typically not equal to $R(t)$. Let

$$c = R_b(t)/R(t) \tag{1}$$

and the vapor bubble volume $V_b(t)$ can be expressed as

$$V_b(t) = \frac{4\pi}{3} R^3(t) f(c), \tag{2}$$

where $f(c)$ depends on the geometry of the truncated sphere. In the limit $c \to 1$, the bubble is a hemisphere and $V_b(t) \to (2\pi/3)R^3(t)$. In the limit $c \to 0$, the bubble approaches a sphere and $V_b(t) \to (4\pi/3)R^3(t)$.

To better focus the effort of the present study on understanding the complex interaction of the thermal field around the vapor dome, additional simplification is introduced. The bubble shape is assumed to be hemispherical ($c = 1$) during the growth. Comparing with the direct numerical simulation technique which solves bubble shape and fluid velocity field using Navier–Stokes equation, this simplification introduces some error in the bubble shape and fluid velocity and temperature fields in this study. However, the hemispherical bubble assumption is generally valid at high Jacob number nucleate boiling (Mei et al., 1995a) and at the early stage of low Jacob number bubble growth (Yaddanapudi and Kim, 2001). A more complete model that incorporates the bubble shape variation could have been used, as in Mei et al. (1995a); however, the present model allows for a great simplification in revealing and presenting the existence and the effects of a thin unsteady liquid thermal boundary layer adjacent to the bubble dome and the influence of bulk liquid thermal boundary layer on saturated nucleate boiling. The present simplified model is not quantitatively valid when the shape of the vapor bubble deviates significantly from a hemisphere.

The energy balance at the liquid–vapor interface for the growing bubble depicted in Fig. 1 is described as

$$\rho_v h_{fg} \frac{dV_b}{dt} = \int -k_l \frac{\partial T_{ml}}{\partial n}\bigg|_{z=L(r)} dA_m + \int -k_l \frac{\partial T_l}{\partial n}\bigg|_{R'=R(t)} dA_b, \tag{3}$$

where ρ_v is the vapor density, h_{fg} is the latent heat, k_l is the liquid thermal conductivity, T_l is the temperature of the bulk liquid, T_{ml} is the temperature of the microlayer liquid, A_m is the area of wedge, A_b is the area of the vapor bubble dome exposed to bulk liquid, $\partial/\partial n$ is the differentiation along the outward normal at the interface, and R' is the spherical coordinate in the radial direction attached to the moving bubble. Eq. (3) simply states that the energy conducted from the liquid to the bubble is used to vaporize the surrounding liquid and thus expand the bubble.

2.2. Microlayer

The microlayer is assumed to be a wedge centered at $r = 0$ with local thickness $L(r)$. Because the hydrodynamics inside the microlayer are not considered, the microlayer wedge angle ϕ cannot be determined as part of the solution. In Cooper and Lloyd (1969), the angle ϕ was related to the viscous diffusion length of the liquid as $R_b(t)\tan\phi = c_1\sqrt{\nu_l t}$ in which ν_l is the kinematic viscosity of the liquid. A small ϕ results in

$$\phi = \frac{c_1\sqrt{\nu_l t}}{R_b(t)}. \tag{4}$$

Cooper and Lloyd (1969) estimated c_1 to be within 0.3–1.0 for their experimental conditions.

A systematic investigation for saturated boiling by Mei et al. (1995b) established that the temperature profile in the liquid microlayer can be taken as linear for practical purposes. The following linear liquid temperature profile in the microlayer is thus adopted in this study

$$T_l(r,z,t) = T_{sat} + \Delta T_{sat}(r,t)\left(1 - \frac{z}{L(r)}\right), \tag{5}$$

where $\Delta T_{sat}(r,t) = T_s(r, z=0, t) - T_{sat}$ and T_s is the temperature of the solid heater.

2.3. Solid heater

The temperature of the solid heater is governed by the energy equation, which is coupled with the microlayer and bulk liquid energy equations. Solid heater temperature variation significantly influences the heat flux into the rapidly growing bubble (Mei et al., 1995a,b). However, in this study, constant wall temperature is assumed so that the case of Yaddanapudi and Kim (2001) can be directly simulated. Thus,

$$\Delta T_{sat}(r,t) = \Delta T_{sat} = T_w - T_{sat}, \tag{6}$$

which can be directly used in Eq. (5) to determine the microlayer temperature profile.

2.4. On the bulk liquid

It was assumed that the vapor bubble is hemispherical in Section 2.1. Furthermore, the velocity and temperature fields are assumed axisymmetric. Unless otherwise mentioned, spherical coordinates (R', ψ, φ), as shown in Fig. 2, are employed for the bulk liquid.

2.4.1. Velocity field

Since there is no strong mean flow over the bubble, the bulk liquid flow induced by the growth of the bubble is mainly of inviscid nature. Thus the liquid velocity field may be determined by solving the Laplace equation $\nabla^2 \Phi = 0$ for the velocity potential Φ. In spherical coordinates, the velocity components are simply given by the expansion of the hemispherical bubble as

$$u_{R'} = \frac{\mathrm{d}R(t)}{\mathrm{d}t}\left(\frac{R(t)}{R'}\right)^2 = \dot{R}\left(\frac{R}{R'}\right)^2, \quad u_\psi = 0, \quad u_\varphi = 0, \tag{7}$$

where $\dot{R} = \frac{\mathrm{d}R(t)}{\mathrm{d}t}$.

2.4.2. Temperature field

By assuming axisymmetry for the temperature fields and using the liquid velocity from Eq. (7), the unsteady energy equation for the bulk liquid in spherical coordinates is

$$\frac{\partial T_\mathrm{l}}{\partial t} + u_{R'}\frac{\partial T_\mathrm{l}}{\partial R'} = \alpha_\mathrm{l}\left(\frac{1}{R'^2}\frac{\partial}{\partial R'}\left(R'^2\frac{\partial T_\mathrm{l}}{\partial R'}\right) + \frac{1}{R'^2\sin\psi}\frac{\partial}{\partial\psi}\left(\sin\psi\frac{\partial T_\mathrm{l}}{\partial\psi}\right)\right). \tag{8}$$

The boundary conditions are

$$\frac{\partial T_\mathrm{l}}{\partial\psi} = 0 \quad \text{at } \psi = 0, \tag{9}$$

$$T_\mathrm{l} = T_\mathrm{s} \quad \text{at } \psi = \frac{\pi}{2}, \tag{10}$$

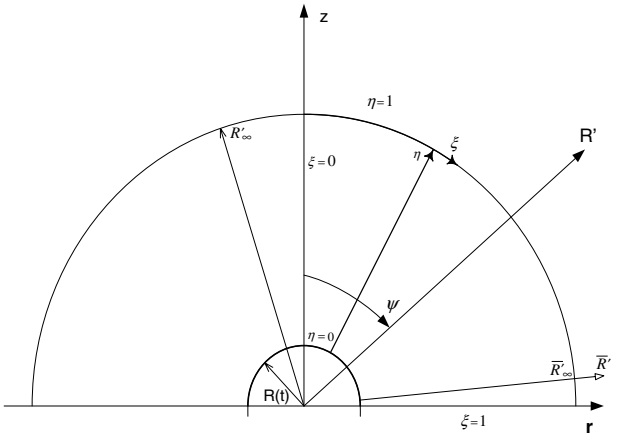

Fig. 2. Coordinate system for the background bulk liquid.

$$T_\mathrm{l} = T_\mathrm{sat} \quad \text{at } R' = R(t), \tag{11}$$

$$T_\mathrm{l} = T_\infty(\psi, t) \quad \text{at } R' \to \infty, \tag{12}$$

where T_∞ is the far field temperature distribution.

To facilitate an accurate computation and obtain a better understanding on the physics of the problem, the following dimensionless variables are introduced,

$$\tau = \frac{t}{t_\mathrm{c}}, \quad \overline{R}' = \frac{R'}{R}, \quad \theta_\mathrm{l} = \frac{T_\mathrm{l} - T_\mathrm{b}}{T_\mathrm{w} - T_\mathrm{b}}, \tag{13}$$

where t_c is a characteristic time chosen to be the bubble departure time, T_w is the initial solid temperature at the solid–liquid interface, and T_b is the bulk liquid temperature far away from the wall, which equals T_sat for saturated boiling.

Using Eq. (7) and Eq. (13), Eq. (8) can be written as

$$\frac{R}{t_\mathrm{c}\dot{R}}\frac{\partial\theta_\mathrm{l}}{\partial\tau} + \left(\frac{1}{\overline{R}'^2} - \overline{R}'\right)\frac{\partial\theta_\mathrm{l}}{\partial\overline{R}'} = \frac{\alpha_\mathrm{l}}{R\dot{R}}\left(\frac{1}{\overline{R}'^2}\frac{\partial}{\partial\overline{R}'}\left(\overline{R}'^2\frac{\partial\theta_\mathrm{l}}{\partial\overline{R}'}\right)\right) + \frac{\alpha_\mathrm{l}}{R\dot{R}}\frac{1}{\sin\psi}\frac{1}{\overline{R}'^2}\frac{\partial}{\partial\psi}\left(\sin\psi\frac{\partial\theta_\mathrm{l}}{\partial\psi}\right). \tag{14}$$

In this equation, the first term on the left-hand-side (LHS) is the unsteady term, and the second term is due to convection in a coordinate system that is attached to the expanding bubble. The right-hand-side (RHS) terms are due to thermal diffusion.

As shown in Chen et al. (1996) and below, the solution for θ_l near $\overline{R} = 1$ possesses a thin boundary layer when $\frac{R\dot{R}}{\alpha_\mathrm{l}} \gg 1$. Therefore, to obtain the accurate heat transfer between the bubble and the bulk liquid, high resolution in the thin boundary layer is essential. Hence, the following grid stretching in the bulk liquid region is applied,

$$\begin{aligned}&\overline{R}' = 1 + (\overline{R}'_\infty - 1)\{1 - S_{\overline{R}'}\tan^{-1}[(1-\eta)\tan(1/S_{\overline{R}'})]\} \quad \text{for } 0 \leqslant \eta \leqslant 1,\\ &\psi = \tfrac{\pi}{2}S_\psi\tan^{-1}[\xi\tan(1/S_\psi)] \quad \text{for } 0 \leqslant \xi \leqslant 1,\end{aligned} \tag{15}$$

where $S_{\overline{R}'}$ and S_ψ are parameters that determine the grid density distribution in the physical domain and $\overline{R}'_\infty = \frac{R'_\infty}{R}$ is the far field end of the computational domain along the radial direction.

Typically $S_{\overline{R}'} \sim 0.65$ and $S_\psi \sim 0.73$, and $\overline{R}'_\infty$ ranges from 5 to 25. Fig. 3 shows a typical grid distribution used in this study.

2.4.3. Asymptotic analysis of the bulk liquid temperature field during early stages of growth

To gain a clear understanding on the interaction of the growing bubble with the background superheated bulk liquid thermal boundary layer, an asymptotic analysis for non-dimensional temperature θ_l is presented, following the work of Chen et al. (1996).

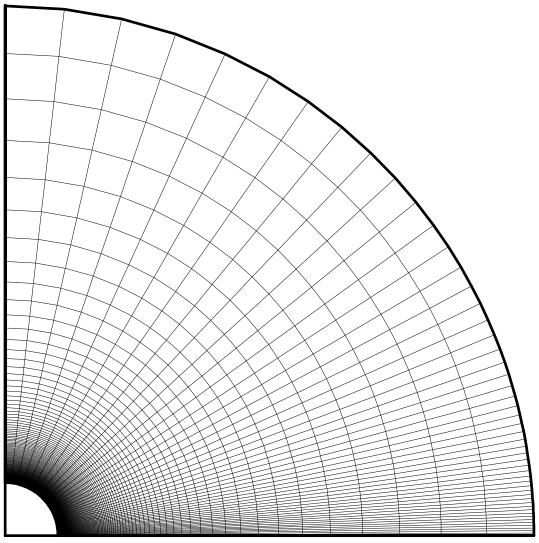

Fig. 3. A typical grid distribution for the bulk liquid thermal field with $S_{\overline{R}'} = 0.65$, $S_\psi = 0.73$ and $\overline{R}'_\infty = 10$.

During the early stages, the bubble growth rate is high and expands rapidly so that

$$A = \frac{R\dot{R}}{\alpha_l} \gg 1. \tag{16}$$

Thus, the solution to Eq. (14) includes an outer approximation in which the thermal diffusion term on the RHS of Eq. (14) is negligible and an inner approximation (boundary layer solution) in which the thermal diffusion balances the convection. Away from the bubble, the outer solution is governed by

$$\frac{R}{\dot{R}}\frac{\partial\theta_l^{\text{out}}}{\partial t} + \left(\frac{1}{\overline{R}'^2} - \overline{R}'\right)\frac{\partial\theta_l^{\text{out}}}{\partial\overline{R}'} = 0, \tag{17}$$

where θ_l^{out} is the outer solution for θ_l in the bulk liquid. The general solution for Eq. (17) is

$$\theta_l^{\text{out}} = F(R(t)(\overline{R}'^3 - 1)^{1/3}), \tag{18}$$

as given in Chen et al. (1996). In the above F is an arbitrary function and it is determined from the initial condition of θ_l or the temperature profile in the background bulk liquid thermal boundary layer. It is noted that the solution for θ_l^{out} is described by $R(t)(\overline{R}'^3 - 1)^{1/3} = \text{const}$ along the characteristic curve.

The initial temperature profile is often written as $\theta_0 = f(\frac{z}{\delta})$. The solution of Eq. (17) is thus expressed as

$$\theta_l^{\text{out}} = f\left\{\frac{R_0\cos\psi}{\delta}\left[1 + \frac{R^3}{R_0^3}(\overline{R}'^3 - 1)\right]^{1/3}\right\}, \tag{19}$$

where R_0 is the initial bubble radius at $t = t_0 \ll t_c$. Provided the bubble growth rate is high, i.e. $A \gg 1$, Eq. (19) is not only an accurate outer solution for the temperature field outside a rapidly expanding bubble, but it is also a good approximation for the far field boundary condition for Eq. (12).

Near the bubble surface, there exists a large temperature gradient between the saturation temperature on the bubble surface and the temperature of the surrounding superheated liquid over a thin region. Therefore, the effect of heat conduction is no longer negligible in this thin region and must be properly accounted for. For a large value of A, a boundary layer coordinate X is introduced,

$$X = \frac{\overline{R}' - 1}{\delta^*(A)}, \tag{20}$$

where $\delta^*(A) \ll 1$ is the dimensionless length scale of the unsteady thermal boundary layer. Substituting Eq. (20) into Eq. (14) results in

$$\begin{aligned}&\frac{R}{t_c\dot{R}}\frac{\partial\theta_l^{\text{in}}}{\partial\tau} + \frac{R}{t_c\dot{R}}\frac{\partial X}{\partial\tau}\frac{\partial\theta_l^{\text{in}}}{\partial X} \\ &\quad + \left(\frac{1}{(1+\delta^*X)^2} - (1+\delta^*X)\right)\frac{1}{\delta^*}\frac{\partial\theta_l^{\text{in}}}{\partial X} \\ &= \frac{1}{A\delta^{*2}}\left(\frac{\partial^2\theta_l^{\text{in}}}{\partial X^2} + \frac{2\delta^*}{1+\delta^*X}\frac{\partial\theta_l^{\text{in}}}{\partial X}\right) \\ &\quad + \frac{1}{A}\frac{1}{(1+\delta^*X)^2}\frac{1}{\sin\psi}\frac{\partial}{\partial\psi}\left(\sin\psi\frac{\partial\theta_l^{\text{in}}}{\partial\psi}\right).\end{aligned} \tag{21}$$

Neglecting higher order terms, Eq. (21) becomes

$$\frac{R}{t_c\dot{R}}\frac{\partial\theta_l^{\text{in}}}{\partial\tau} = \frac{1}{A\delta^{*2}}\frac{\partial^2\theta_l^{\text{in}}}{\partial X^2} + 3X\left(1 - \frac{R}{3t_c\dot{R}X}\frac{\partial X}{\partial\tau}\right)\frac{\partial\theta_l^{\text{in}}}{\partial X}. \tag{22}$$

The balance between the convection term and the diffusion term on the RHS of Eq. (22) requires

$$\delta^* = A^{-1/2} = \left(\frac{R\dot{R}}{\alpha_l}\right)^{-1/2}. \tag{23}$$

Hence Eq. (22) becomes

$$\frac{R}{t_c\dot{R}}\frac{\partial\theta_l^{\text{in}}}{\partial\tau} = \frac{\partial^2\theta_l^{\text{in}}}{\partial X^2} + \left(3 - \frac{R}{2t_c\dot{R}}\frac{\dot{A}}{A}\right)X\frac{\partial\theta_l^{\text{in}}}{\partial X}. \tag{24}$$

The boundary conditions for the inner (boundary layer) solution are

$$\theta_l^{\text{in}} = \theta_{\text{sat}} = \frac{T_{\text{sat}} - T_b}{T_w - T_b} \quad \text{at } X = 0, \tag{25}$$

$$\theta_l^{\text{in}} = 1 \quad \text{at } X \to \infty. \tag{26}$$

For $\tau \ll 1$, $R(t) \propto t^{1/2}$ and $\frac{R}{t_c\dot{R}} \approx \tau$. Thus, the LHS of Eq. (24) is small and can also be neglected. Eq. (24) then reduces to

$$\frac{\partial^2\theta_l^{\text{in}}}{\partial X^2} + 3X\frac{\partial\theta_l^{\text{in}}}{\partial X} = 0 \quad \text{for } \tau \ll 1. \tag{27}$$

The solution for Eq. (27) is

$$\theta_l^{\text{in}} = (1 - \theta_{\text{sat}})\text{erf}\left(\sqrt{\frac{3}{2}}X\right) + \theta_{\text{sat}}. \tag{28}$$

For $\tau \ll 1$, by matching the outer and inner solutions given by Eqs. (19) and (28), the uniformly valid asymptotic solution of the bulk liquid temperature for the saturated boiling problem considered here is obtained,

$$\theta_l = f\left\{\frac{R_0\cos\psi}{\delta}\left[1+\frac{R^3}{R_0^3}\left(\overline{R}'^3-1\right)\right]^{1/3}\right\} + (\theta_{sat}-1)\mathrm{erfc}\left(\sqrt{\frac{3}{2}}X\right), \quad (29)$$

where $\theta_{sat}=\frac{T_{sat}-T_b}{T_w-T_b}$ and *erfc* is the complimentary error function. Eq. (29) is an asymptotic solution for θ_l valid for $\tau \ll 1$.

The asymptotic solution given by Eq. (29) for the liquid thermal field provides an analytical framework to understand: (1) how the temperature field of background superheated bulk liquid boundary layer influences the temperature θ_l near the vapor bubble through the function f; (2) how the bubble growth $R(t)$ and liquid thermal diffusivity affect the liquid thermal field θ_l through the rescaled inner variable X as defined in Eqs. (20) and (23); and (3) how the folding of the temperature contours near the bubble occurs through the dependence of $\cos\psi$ term in Eq. (29). More importantly, from a computational standpoint, it provides: (1) an accurate measure on the thickness of the rapidly moving thermal boundary layer; and (2) a reliable guideline for estimating the adequacy of computational resolution in order to obtain an accurate assessment of heat transfer to the bubble.

2.5. Initial conditions

The computation must start from a very small but non-zero initial time τ_0, so that $\overline{R}(\tau_0)$ is sufficiently small at the initial stage. To obtain enough temporal resolution for the initial rapid growth stage and to save computational effort for the later stage, the following transformation is used,

$$\tau = \sigma^2. \quad (30)$$

Thus a constant "time step" $\Delta\sigma$ can be used in the computation.

The initial temperature profile inside the superheated bulk liquid thermal boundary layer plays an important role to the solution of θ_l, which in turn affects the heat transfer to the bubble through the dome.

There exist both experimental and theoretical studies that have considered the bulk liquid temperature profile in the vicinity of a vapor bubble. Hsu (1962) estimated the temperature profile of the superheated thermal layer adjacent to the heater surface and found the layer to be quite thin; thus the temperature gradient inside the thermal layer is almost linear. However, beyond the superheated layer the temperature is held essentially constant at the bulk temperature due to strong turbulent convection. The experimental study by Wiebe and Judd (1971) revealed similar results. It was found that the superheated bulk liquid thermal boundary layer thickness, δ, decreases with increasing wall heat flux due to enhanced turbulent convection. A high wall heat flux results in increased bubble generation, and the bulk liquid is stirred more rapidly by growing and departing vapor bubbles. To estimate the superheated layer thickness, Hsu (1962) used a thermal diffusion model within the bulk liquid. Han and Griffith (1965) used a similar model and estimated the thickness to be

$$\delta = \sqrt{\pi\alpha_l t_w}, \quad (31)$$

where t_w is the waiting period. The thermal diffusion model often over-estimates the thermal layer thickness, as it neglects the turbulent convection, which is quite strong as reported by Hsu (1962) and Wiebe and Judd (1971).

Generally, the bulk liquid temperature profile is almost linear inside the superheated thermal boundary layer, and remains essentially uniform at the bulk temperature T_b beyond the superheated background thermal boundary layer. Accordingly, the initial condition for the bulk liquid thermal field used in the numerical solution is given by

$$\theta_0 = \begin{cases} 1-\frac{z}{\delta}, & z<\delta, \\ 0, & z \geqslant \delta. \end{cases} \quad (32)$$

In the asymptotic solution, the discontinuity of $\partial\theta_l/\partial z$ in the above profile causes the solution for θ_l to be discontinuous. For clarity, the following exponential profile is employed in representing the asymptotic solution

$$\theta_0 = \exp\left(-\frac{z}{\delta}\right). \quad (33)$$

2.6. Solution procedure

An Euler backward scheme is used to solve Eq. (14). A second-order upwind scheme is used for the convection term and a central difference scheme is used for the thermal diffusion terms.

After the bulk liquid temperature field is obtained, the solid heater temperature field is solved, and the bubble radius $R(\tau)$ is updated using Eq. (3) and Euler's explicit scheme. The information for $R(\tau)$ is a necessary input in Eq. (14). Although the solution for $R(\tau)$ is only first-order accurate in time, the $O(\Delta\tau)$ accuracy is not a concern here because a very small $\Delta\tau$ has to be used to ensure sufficient resolution during the early stages. Typically, $n = 10^4$ time steps are used.

3. Results and discussion

3.1. Asymptotic structure of liquid thermal field

To gain an analytical understanding of the liquid thermal field near the bubble and to validate the accuracy of the computational treatment for the thin unsteady thermal boundary layer, comparison between the computational and the asymptotic solutions for θ_l near the bubble surface is first presented. As mentioned previously, the validity of the outer solution of the asymptotic analysis only requires $A \gg 1$, which is satisfied under most conditions due to rapid vapor bubble growth. The inner solution is valid for $\tau \ll 1$ in addition to $A \gg 1$.

The comparison is presented for bubble growth in saturated liquid with $A = 14000$. The initial temperature profile follows Eq. (33) and $\frac{\delta}{R_c} = 0.5$, in which R_c is the bubble radius at t_c. There are 200 and 50 grid intervals along the R'- and ψ-directions, respectively. The grid stretching factors are $S_{\overline{R}'} = 0.65$ and $S_\psi = 0.73$ for the computational case.

Fig. 4 compares the temperature profiles between the asymptotic and numerical solutions at $\tau = 0.001$, 0.01, 0.1, and 0.3 for $\psi = 0°$, 40°, and 71°. There are two important points to be noted. First of all, it is seen that the temperature gradient is indeed very large near the bubble surface because the unsteady thermal boundary layer is very thin. Secondly, numerical solutions agree very well with the asymptotic solutions at $\tau = 0.001$ and 0.01. The excellent agreement between the numerical and analytical solutions indicates that the numerical treatment in this study is correct. At $\tau = 0.1$ and 0.3, the asymptotic inner solution given by Eq. (29) is no longer accurate, while the outer solution remains valid because $A \gg 1$ is the only requirement. At $\tau = 0.1$ and 0.3 the numerical solution matches very well with the outer solution. This again demonstrates the integrity of the present numerical solution over the entire domain due to sufficient computational resolution near the bubble surface and removal of undesirable numerical diffusion through the use of second-order upwind scheme in the radial direction for Eq. (14).

The large temperature gradient near the dome causes high heat transfer from the superheated liquid to the vapor bubble through the dome. This large gradient results from the strong convection effect that is caused

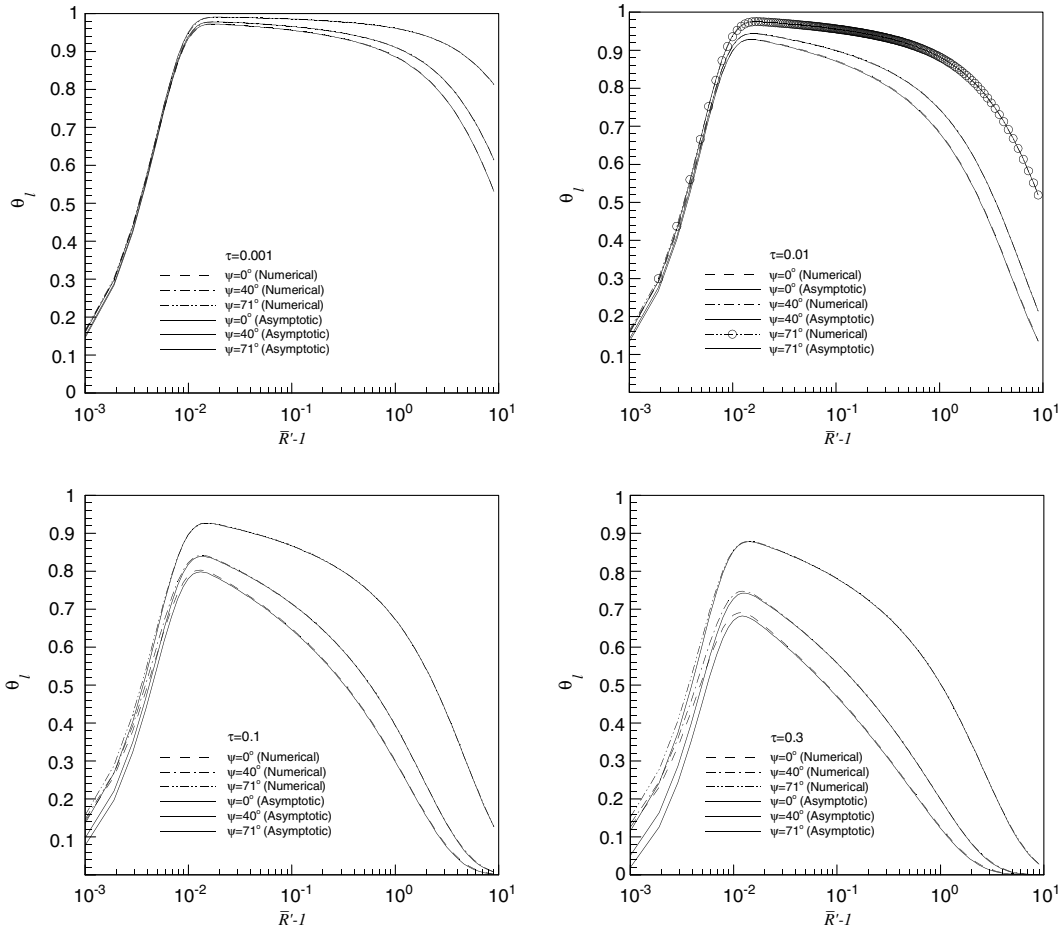

Fig. 4. Comparison of the asymptotic and the numerical solutions at $\tau = 0.001$, 0.01, 0.1 and 0.3 for $\psi = 0°$, 40°, and 71°.

by the rapid bubble growth (see Eq. (14) for the origin in the governing equation and Eq. (19) for the explicit dependence on the bubble growth). Thus the bulk liquid in the superheated boundary layer supplies a sufficient amount of energy to the bubble.

To capture the dynamics of the unsteady boundary layer, a sufficient number of computational grids is required inside this layer. The asymptotic analysis gives an estimate for the unsteady boundary layer thickness on the order of $\delta^* \sim \frac{3}{\sqrt{14000}} = 0.025$, which agrees with the numerical solution in Fig. 4. At $\tau = 0.01$ in Fig. 4, the discrete numerical results are presented. There are about 23 points inside the layer of thickness $\delta^* = 0.025$. This provides sufficient resolution for the temperature profile in the unsteady thermal boundary layer. In contrast, most computational studies on the thermal field around the bubble dome reported in the open literature have insufficient grid resolution adjacent the dome, which leads to an inaccurate heat transfer assessment.

Fig. 5 shows the effect of parameter A on the asymptotic solution. When A is large, the asymptotic and numerical solutions agree very well. The discrepancy between asymptotic and numerical solutions inside the unsteady thermal boundary layer increases when A decreases. However, the outer solution remains valid for the far field even when A becomes small.

The temperature contours shown in Fig. 6 are difficult to obtain experimentally. Only recent progress in holographic thermography permits such measurements. Ellion (1954) has stated that there exists an unsteady thermal boundary layer contiguous to the vapor bubble during the bubble growth. Recently, Mayinger (1996) used a holography technique to capture the folding of the temperature contours during subcooled nucleate boiling. Although his study considered subcooled nucleate boiling, the pattern of the temperature distribution near the bubble dome by Mayinger (1996) is very similar to that shown in the Fig. 6. It is expected that experimental evidence of contour folding in saturated nucleate boiling will be reported in the future.

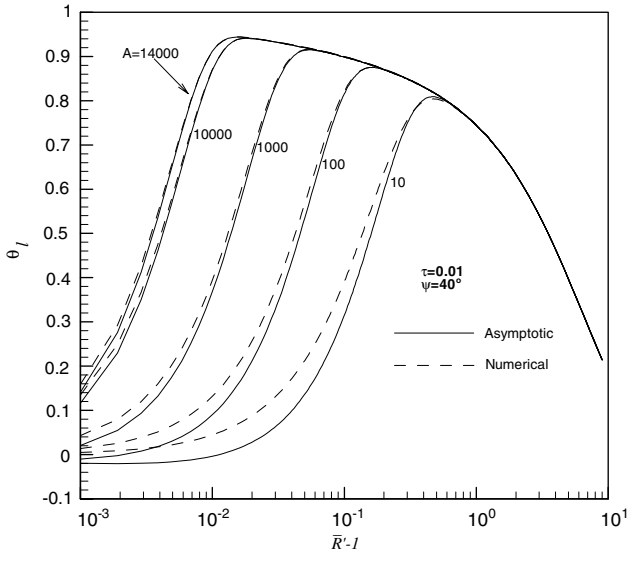

Fig. 5. Effect of parameter A on the liquid temperature profile near bubble.

3.2. Constant heater temperature bubble growth in the experiment of Yaddanapudi and Kim (2001)

In the experiment of Yaddanapudi and Kim (2001), single bubbles growing on a heater array kept at nominally constant temperature were studied. The liquid used is FC-72, and the wall superheat is maintained at 22.5 °C, so that Jacob number is 39. The bubble shape in the early stage appears to be hemispherical. To calculate the heat flux from the microlayer to the vapor bubble in the present model, the microlayer wedge angle ϕ or constant c_1 in Eq. (4) must be determined. Neither ϕ nor c_1 has been measured. However, the authors have reported the amount of wall heat flux from the wall to the bubble through an equivalent bubble diameter d_{eq} assuming that the wall heat flux is the only source of heat entering the bubble. Since in the present model this heat flux is assumed to pass through the microlayer, it may be used to evaluate the constant c_1 via trial and error. The superheated thermal boundary layer thickness δ of the bulk liquid in Eq. (32) is also a required input. The computed growth rate $R(t)$ is matched with the experimentally measured $R(t)$ in order to determine δ. The simulation is carried out only for the early stage of bubble growth. This is because after $t = 6\text{–}8 \times 10^{-4}$ s the base of the bubble does not expand anymore, and the bubble shape deviates from a hemisphere. Furthermore, there is the possibility of the microlayer being dried out in the latter growth stages as a result of maintaining a constant wall temperature, as was observed by Chen et al. (2003).

Fig. 7 shows the computed equivalent bubble diameter $d_{eq}(t)$, together with the experimentally determined equivalent $d_{eq}(t)$. In the present model, d_{eq} is calculated using

$$\rho_v h_{fg} \cdot \frac{dV_b}{dt} = \int -k_l \frac{\partial T_{ml}}{\partial n}\bigg|_{z=L(r)} dA_m, \tag{34}$$

where $V_b = \frac{\pi}{6} d_{eq}^3$. The heat flux includes only that from the microlayer and this allows c_1 to be evaluated. For d_{eq}, to match the measured data as shown in Fig. 7, it requires $c_1 = 3.0$.

Fig. 8 compares the computed bubble diameter $d(t) = 2R(t)$ and those reported by Yaddanapudi and Kim (2001). In Fig. 8, $\delta = 30$ μm is used in addition to $c_1 = 3.0$ in matching the predicted bubble growth with measured data. The good agreement obtained can be partly attributed to the adjustment in the superheated

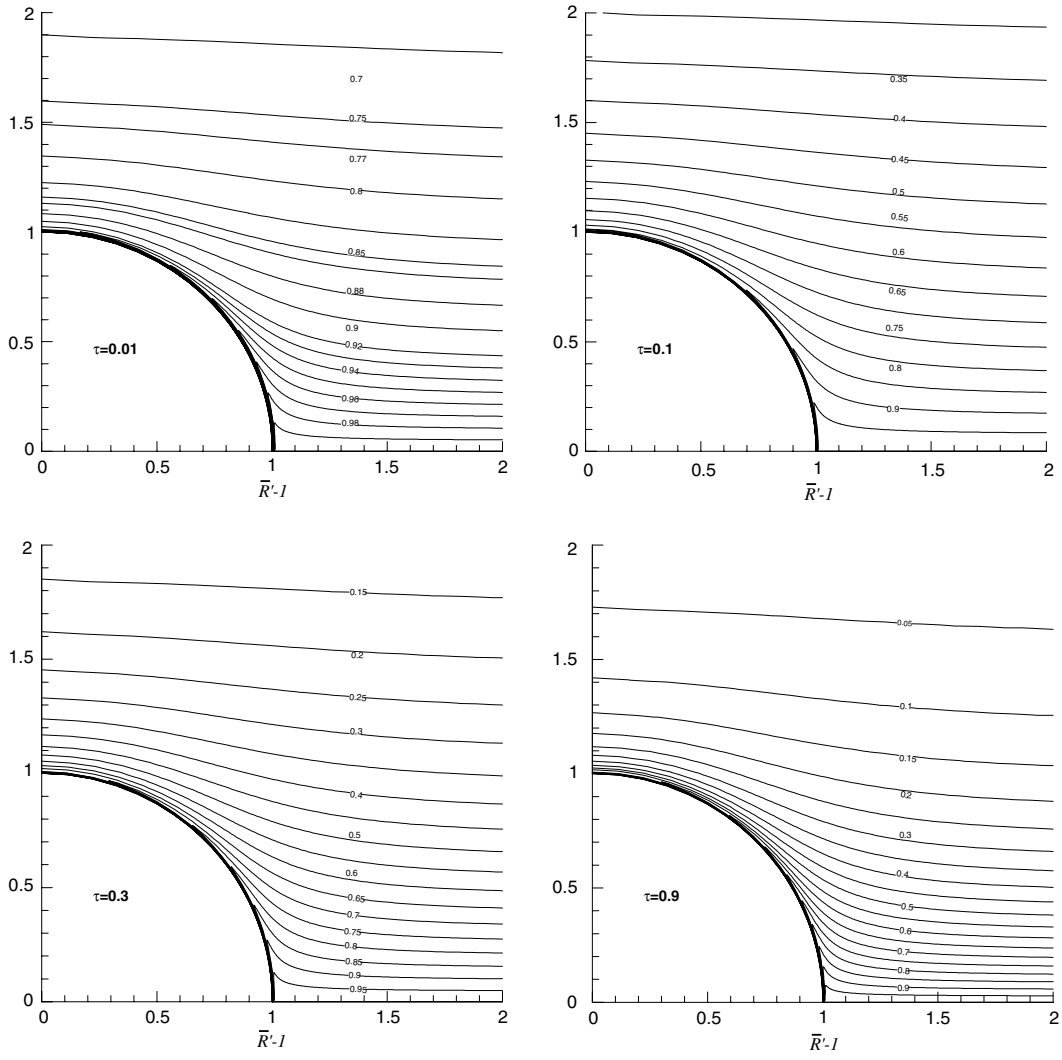

Fig. 6. The computed isotherms near a growing bubble in saturated liquid at $\tau = 0.01$, 0.1, 0.3, and 0.9.

bulk liquid thermal boundary layer thickness δ. Because the heat transfer to the bubble (through the microlayer and through the dome) is of two different mechanisms, the good agreement over the range is an indication of the correct physical representation by the present model.

Fig. 9 shows the total heat entering bubble and the respective contribution from the microlayer and from the unsteady thermal boundary layer. The contribution from the unsteady thermal boundary layer accounts for about 70% of the total heat transfer. It was reported by Yaddanapudi and Kim (2001) that approximately 54% of the total heat is supplied by the microlayer over the entire growth cycle. Since, the simulation is only carried out for the early stage of bubble growth, it is difficult to compare the microlayer contribution to heat transfer reported by Yaddanapudi and Kim (2001) with that predicted by current model. At the end, the bubble expands outside the superheated boundary layer and protrudes into the saturated bulk liquid. The heat transfer from dome thus slows down. Hence, the 54% for the entire bubble growth period dose not contradict a higher percentage of contribution computed from the unsteady thermal boundary layer during the early stages.

Fig. 10 shows the computed temperature contours associated with Yaddanapudi and Kim's (2001) experiment for the estimated δ and c_1. Folding of the temperature contours is clearly observed in the simulation for saturated boiling.

3.3. Effect of bulk liquid thermal boundary layer thickness δ on bubble growth

Since the superheated bulk liquid thermal boundary layer thickness, δ, determines how much heat is stored in the layer, it is instructive to conduct a parametric study on the effects bubble growth with varying δ. All parameters are the same as those used in Yaddanapudi

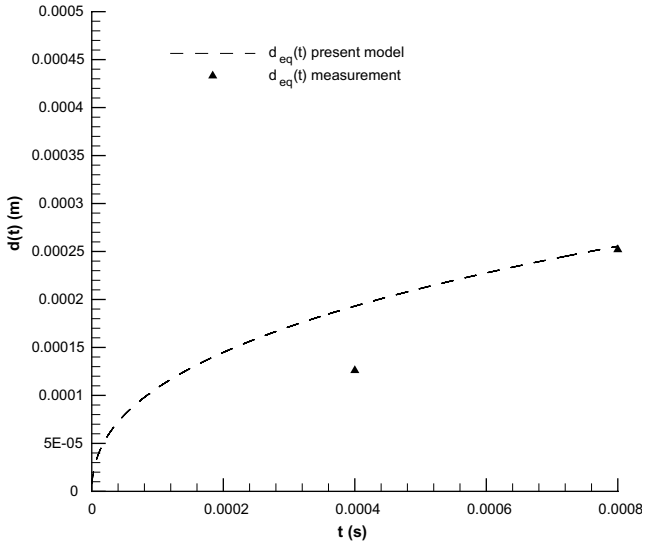

Fig. 7. Comparison of the equivalent bubble diameter d_{eq} for the experimental data of Yaddanapudi and Kim (2001) and that computed for heat transfer through the microlayer ($c_1 = 3.0$).

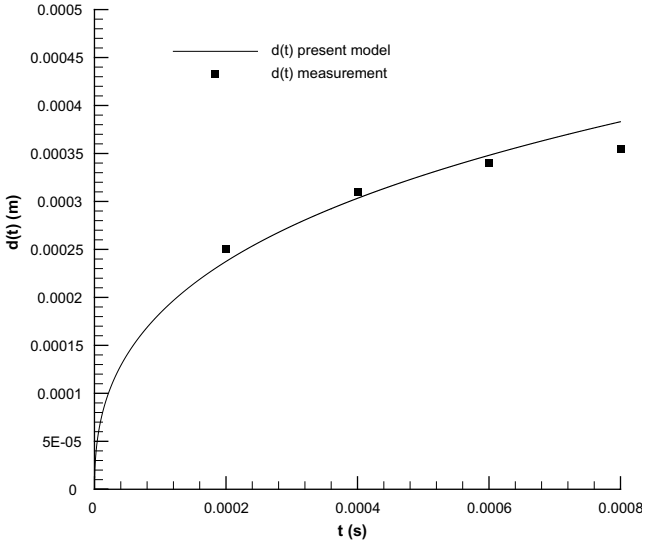

Fig. 8. Comparison of bubble diameter, $d(t)$, between that computed using the present model and the measured data of Yaddanapudi and Kim (2001). Here, $c_1 = 3.0$ and $\delta = 30$ μm.

and Kim's (2001) experiment except that δ is varied. Hence the influence of the superheated thermal boundary layer thickness δ on the bubble growth is elucidated.

Fig. 11 shows the effect on the bubble growth rate of varying δ (from 1 to 100 μm). The thicker the bulk liquid thermal boundary layer, the faster the bubble grows. A large δ implies a larger amount of heat is stored in the background bulk liquid surrounding the bubble. It is also clear that when δ approaches zero, the bubble growth rate becomes unaffected by the variation of δ.

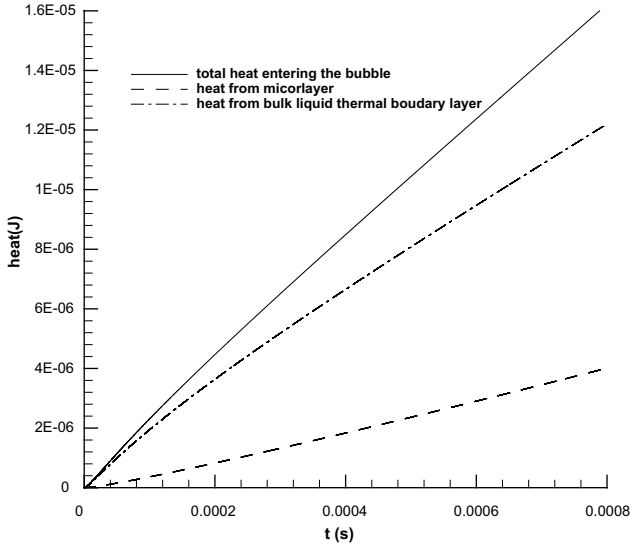

Fig. 9. Comparison between heat transfer to the bubble through the vapor dome and that through the microlayer.

The reason is when δ is small, most of heat supplied for bubble growth comes from the microlayer and the contribution from the dome can be neglected.

It is also noted that for $\delta = 100$ μm, if the bubble eventually grows to about several millimeters, the effect of the bulk liquid thermal boundary layer is negligible on $R(t)$ for most of the growth period except at the very early stages. Physically, this is because the bubble dome is quickly exposed to the saturated bulk liquid so that it is at thermal equilibrium with the surroundings. For small bubbles, it will be immersed inside the thermal boundary layer most of time. Hence the effect of the bulk liquid thermal boundary layer becomes significant for the bubble growth.

The microlayer angle ϕ and the superheated bulk liquid thermal liquid boundary layer thickness δ are the required inputs to compute bubble growth in the present model. However, neither of these parameters is typically measured or reported in bubble growth experiments. It is strongly suggested that the bulk liquid thermal boundary layer thickness δ be measured and reported in future experimental studies. For a single bubble study, δ in the immediate neighborhood of the nucleation site should be measured.

4. Conclusions

In this study, a physical model is presented to predict the early stage bubble growth in saturated heterogeneous nucleate boiling. The thermal interaction of the temperature fields around the growing bubble and vapor bubble together with the microlayer heat transfer is properly considered. The structure of the thin unsteady

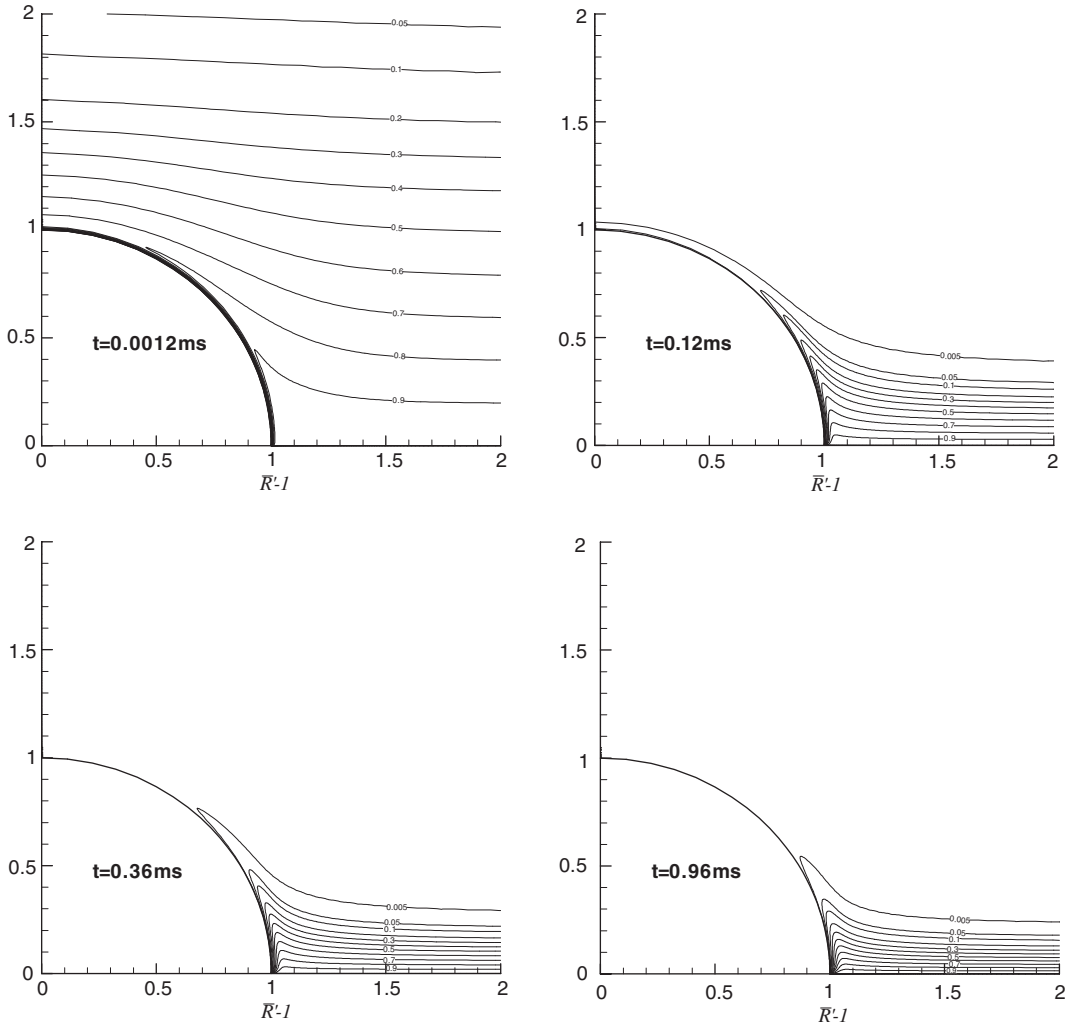

Fig. 10. The computed isotherms in the bulk liquid corresponding to the thermal conditions reported by Yaddanapudi and Kim (2001).

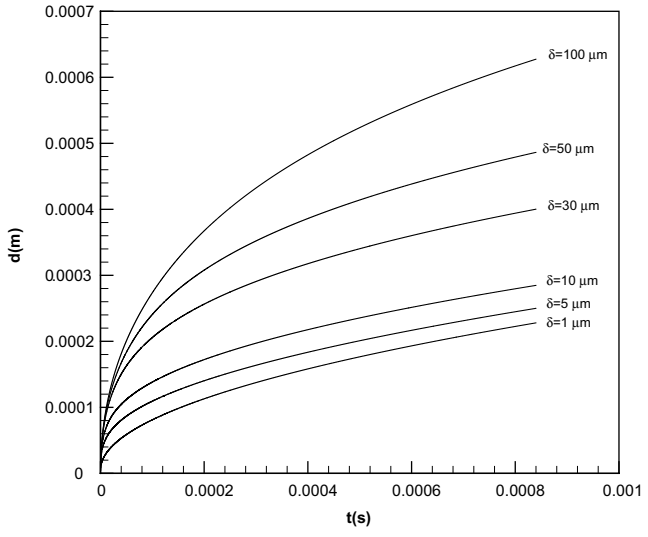

Fig. 11. Effect of bulk liquid thermal boundary layer thickness δ on bubble growth.

liquid thermal boundary layer is revealed by the asymptotic and numerical solutions. The existence of a thin unsteady thermal boundary layer near the rapidly growing bubble allows for a significant amount of heat flux from the bulk liquid to the vapor bubble dome, which in some cases can be larger than the heat transfer from the microlayer. The experimental observation by Yaddanapudi and Kim (2001) on the insufficiency of heat transfer to the bubble through the microlayer is elucidated. For thick superheated thermal boundary layers in the bulk liquid, the heat transfer though the vapor bubble dome can contribute substantially to the vapor bubble growth.

Acknowledgements

This work was supported by NASA Glenn Research Center under contract NAG3-2750 and NASA Kennedy Space Center.

References

Akiyama, M., Tachibana, F., Ogawa, N., 1969. Effect of pressure on bubble growth in pool boiling. Bulletin of JSME 12, 1121–1128.

Bai, Q., Fujita, Y., 2000. Numerical simulation of bubble growth in nucleate boiling—effects of system parameter. In: Engineering Foundation Boiling 2000 Conference, Anchorage AL, May 2000, pp. 116–135.

Chen, T., Klausner, J.F., Chung, J.N., 2003. Subcooled boiling heat transfer and dryout on a constant temperature microheater. In: Proceeding of the 5th International Conference on Boiling Heat Transfer, Montego Bay, Jamaica.

Chen, W., 1995. Vapor bubble growth in heterogeneous boiling. Ph.D Dissertation, University of Florida.

Chen, W., Mei, R., Klausner, J., 1996. Vapor bubble growth in highly subcooled heterogeneous boiling. Convective Flow Boiling, 91–97.

Cooper, M.G., 1969. The microlayer and bubble growth in nucleate pool boiling. International Journal of Heat and Mass Transfer 12, 895–913.

Cooper, M.G., Lloyd, A.J.P., 1969. The microlayer in nucleate pool boiling. International Journal of Heat and Mass Transfer 12, 915–933.

Cooper, M.G., Vijuk, R.M., 1970. Bubble growth in nucleate pool boiling. In: Proceeding of 4th International Heat Transfer Conference, Paris, vol. 5. Elsevier, Amsterdam, p. B2.1.

Ellion, M.E., 1954. A study of the mechanism of boiling heat transfer. Ph.D Thesis, California Institute of Technology.

Fyodorov, M.V., Klimenko, V.V., 1989. Vapour bubble growth in boiling under quasi-stationary heat transfer conditions in a heating wall. International Journal of Heat and Mass Transfer 32, 227–242.

Han, C., Griffith, P., 1965. The mechanism of heat transfer in nucleate pool boiling—part I. International Journal of Heat and Mass Transfer 8, 887–904.

Hsu, Y.Y., 1962. On the size of active nucleation cavities on a heating surface. Journal of Heat Transfer (August), 207–216.

Koffman, L.D., Plesset, M.S., 1983. Experimental observations of microlayer in vapor bubble growth on a heated solid. Journal of Heat Transfer 105, 625–632.

Labunstov, D.A., 1963. Mechanism of vapor bubble growth in boiling under on the heating surface. Journal of Engineering Physics 6 (4), 33–39.

Lee, R.C., Nydahl, J.E., 1989. Numerical calculation of bubble growth in nucleate boiling from inception through departure. Journal of Heat Transfer 111, 474–479.

Mayinger, F., 1996. Advanced experimental methods. Convective Flow Boiling. Taylor & Francis. pp. 15–28.

Mei, R., Chen, W., Klausner, J., 1995a. Vapor bubble growth in heterogeneous boiling—I. Formulation. International Journal of Heat and Mass Transfer 38 (5), 909–919.

Mei, R., Chen, W., Klausner, J., 1995b. Vapor bubble growth in heterogeneous boiling—II. Growth rate and thermal fields. International Journal of Heat and Mass Transfer 38 (5), 921–934.

Moore, F.D., Mesler, R.B., 1961. The measurement of rapid surface temperature fluctuations during nucleate boiling of water. AIChE Journal 7, 620–624.

Son, G., Dhir, V.K., Ramannujapu, N., 1999. Dynamics and heat transfer associated with a single bubble during nucleate boiling on a horizontal surface. Journal of Heat Transfer 121, 623–631.

van Stralen, S.J.D., Cole, R., Sluyter, W.M., Sohal, M.S., 1975a. Bubble growth rates in nucleate boiling of water at subatmospheric pressures. International Journal of Heat and Mass Transfer 18, 655–669.

van Stralen, S.J.D., Sohal, M.S., Cole, R., Sluyter, W.M., 1975b. Bubble growth rates in pure and binary systems: combined effect of relaxation and evaporation microlayer. International Journal of Heat and Mass Transfer 18, 453–467.

van Stralen, S.J.D., 1967. The mechanism of nucleate boiling in pure liquid and in binary mixtures, parts I–IV. International Journal of Heat and Mass Transfer 9, 995–1020, 1021–1046; 10, 1469–1484, 1485–1498.

Wiebe, J.R., Judd, R.L., 1971. Superheat layer thickness measurements in saturated and subcooled nucleate boiling. Journal of Heat Transfer (November), 455–461.

Yaddanapudi, N., Kim, J., 2001. Single bubble heat transfer in saturated pool boiling of FC-72. Multiphase Science and Technology 12 (3–4), 47–63.